4-1-1997

Fragment Rotational Distributions From The Dissociation Of NeBr2: Experimental And Classical Trajectory Studies

Mehdi Nejad-Sattari , '95

Thomas Alex Stephenson
Swarthmore College, tstephe1@swarthmore.edu

Fragment rotational distributions from the dissociation of NeBr 2 : Experimental and classical trajectory studies

Mehdi Nejad-Sattari and Thomas A. Stephenson

Citation: The Journal of Chemical Physics **106**, 5454 (1997); doi: 10.1063/1.473570
View online: http://dx.doi.org/10.1063/1.473570
View Table of Contents: http://scitation.aip.org/content/aip/journal/jcp/106/13?ver=pdfcov
Published by the AIP Publishing

Fragment rotational distributions from the dissociation of $NeBr_2$: Experimental and classical trajectory studies

Mehdi Nejad-Sattari and Thomas A. Stephenson[a)]
Department of Chemistry, Swarthmore College, Swarthmore, Pennsylvania 19081-1397

(Received 21 October 1996; accepted 31 December 1996)

The Br_2 fragment rotational distributions that result from the vibrational predissociation of $NeBr_2$ in the *B* electronic state have been measured for several initial vibrational levels. In each case, the rotational distributions extend to the effective energetic limit determined by the amount of energy available (E_{avl}) for disposal into the fragment rotational and translational degrees of freedom. Analysis of the data allows refinement of the $NeBr_2$ dissociation energy; we find that $D_0 = 70.0 \pm 1.1\ cm^{-1}$ for the *X* electronic state, $v = 0$. Both $\Delta v = -1$ and -2 dissociation events have been examined. For dissociation pathways with approximately the same value of E_{avl} the $\Delta v = -2$ pathways are observed to have a higher fraction of the fragment energy in rotational excitation. The overall shape of the $\Delta v = -1$ distributions are insensitive to the value of E_{avl}, suggesting that a Franck–Condon model for the dissociation may have some validity, though quantitative quantum mechanical calculations demonstrate that this model does not reproduce the large degree of fragment rotational excitation. Two classical models for the dissociation also fail to reproduce the extent of fragment rotational distribution. This result is discussed in light of previous experimental and theoretical investigations, focusing on the apparent agreement of classical models with the IBr fragment rotational distributions that result from the dissociation of NeIBr. © *1997 American Institute of Physics.* [S0021-9606(97)02013-8]

I. INTRODUCTION

Photodissociation fragment rotational distributions have proven to be an important experimental diagnostic of the depth and anisotropy of intermolecular potential energy surfaces, along with providing insights into the mechanism of elementary fragmentation events.[1,2] As prototype systems for more traditional chemically bound molecules, studies of the fragmentation of rare gas–halogen van der Waals molecules have occupied an important place in this field. The result of over two decades of experimental investigations has been a large number of binding energies, equilibrium geometries, empirical potential energy surfaces, and fragment product rotational and vibrational state distributions.[3] This experimental activity has been accompanied by significant theoretical investigations that have in some cases prompted more and better experimental measurements.[4–19]

Experimental studies of diatomic halogen fragment internal state distributions date to the pioneering work by Levy and co-workers on rare gas–I_2 complexes in the late 1970's.[20] In this work, dispersed fluorescence was used to measure I_2 fragment vibrational distributions. More recently, Lester and co-workers used pump–probe techniques to examine the ICl rotational and vibrational distributions that result from the fragmentation of NeICl[21–24] and HeICl.[21,25] Janda and co-workers have expanded on this development in their elegant and detailed studies of rare gas–Cl_2[26–32] and $HeBr_2$[33,34] complexes and we have reported on the fragment rotational distributions from NeIBr in a previous report from this laboratory.[35] Even with relatively simple excited state rare gas–halogen interaction potentials (often represented as a sum of atom–atom pair potentials), quantum mechanical simulations of fragment rotational distributions are in reasonable agreement with the experimental measurements on rare gas–ICl[8,9,13] and rare gas–Cl_2[5–7,9–11,17] complexes.

One of the striking discrepancies in the experimental and theoretical results to data has been the relevance and utility of classical simulations to understanding the dissociation of rare gas–halogen complexes. Drobits and Lester found that the quantum number for the ICl rotational level most populated (in the dissociation of NeICl) varies linearly with the square root of the total fragment energy; the similarity of this dependence to that derived from the application of classical inelastic scattering concepts was noted.[24] Extending these ideas, Waterland *et al.* investigated the semiclassical dynamics of the HeICl molecule and found that features in the rotational distribution could be identified as classical rotational rainbows.[25] Quantum mechanical calculations performed on HeICl confirm the general premise of the classical models, i.e., that final state interactions between the recoiling fragments and not initial state preparation or the quantum dynamics associated with vibrational coupling dominate the formation of rotationally excited fragments.[8] Most recently, we have found that the semiclassical approach taken by Waterland *et al.* provides an excellent fit to the IBr fragment rotational distribution from the dissociation of NeIBr.[35]

Contradicting these results, Janda and co-workers find that the dynamics of the rare gas–Cl_2 complexes are consistent only with quantum mechanical calculations. Specifically, for $NeCl_2$, the rotational distributions are insensitive to the total energy available for disposal into the translational and rotational degrees of freedom (E_{avl}), suggesting that

a)Author to whom correspondence should be addressed.

 0021-9606/97/106(13)/5454/14/$10.00

classical scattering concepts are inappropriate for this molecule.[28] Cline *et al.* suggest that a Franck–Condon model—in which the rotational distribution is derived from a projection of the initial bending state wave function onto the fragment diatomic rotational states—is consistent with this insensitivity to E_{avl}.[28] These workers note, however, that the Franck–Condon model does not account for other features of the observed distributions, such as their bimodal character. Three-dimensional quantum mechanical calculations do reproduce the essential features of the fragment distributions that result from the fragmentation of $NeCl_2$ (Ref. 28) and $HeCl_2$.[26] Additional experimental and theoretical studies have demonstrated that intramolecular vibrational redistribution is an important part of the dynamics of $ArCl_2$ and is further evidence that neglect of the quantum dynamics of the vibrational energy redistribution that must precede dissociation can be a serious omission.[6,10,17,30]

These conflicting results present an ambiguous picture of the photofragmentation of rare gas–halogen van der Waals molecules. A central uncertainty is the limits of the validity of ''classical'' concepts in modeling the dissociation and extracting quantum state distributions. Attempts to develop intuitive physical models for these processes—and by extension more general photofragmentation reactions—rely on an understanding of this issue and has provided the motivation for our current investigation. Specifically, with the light, homonuclear Cl_2 and the heavy, heteronuclear IBr fragments providing extreme examples in the application of classical concepts to the dissociation of rare gas–halogen complexes, we sought to reexamine the vibrational predissociation dynamics of $NeBr_2$ in the B electronic state.

The $NeBr_2$ van der Waals molecule was first observed by Swartz *et al.* using laser-induced fluorescence excitation spectroscopy.[36] Vibrational levels $v=11$–30 in the B electronic state were observed; the shape of the excitation features were consistent with a T-shaped geometry for the complex. Based on an analysis of the homogeneous width of the $NeBr_2$ transitions, the vibrational predissociation lifetimes were found to decrease with increasing vibrational quantum number in a manner that is consistent with the ''energy gap'' or ''momentum gap'' relations.[36] In a higher resolution experiment, Thommen *et al.* resolved the rotational structure associated with the (10,0) $B \leftarrow X$ transition in $NeBr_2$ and demonstrated conclusively that the molecule assumes a T-shaped geometry.[37] A lifetime of 355 ps was determined from an analysis of the homogeneous linewidth of the features observed.

The Br_2 fragment quantum state distribution that results from the dissociation of $NeBr_2$ was measured by Cline *et al.* using the dispersed fluorescence technique.[38] They find that for B state vibrational levels with $v<27$, $\Delta v=-1$ dissociation processes dominate the dynamics. Analysis of the observed rotational contours in terms of a Boltzmann distribution for the quantum state populations reveals that little of the available energy is channeled into fragment rotation. In a separate investigation, Sivakumar *et al.* examined the rotational distribution that results from the dissociation of $NeBr_2$ using two-color pump–probe laser-induced fluorescence spectroscopy.[39] The focus in this work was on complexes excited to $v=10$ of the B electronic state, which generate Br_2 fragments in $v=9$. In these experiments, the probe laser had a bandwidth that was too large to cleanly resolve the rotational structure, so no attempt was made to assign independent populations to individual fragment rotational states. A Boltzmann distribution of rotational populations ($T=6.9$ K) was found to reproduce the photofragment excitation spectrum within the resolution of the experimental data. This temperature corresponds to an average fragment rotational energy of 5 cm^{-1}, a result that is small compared to the 70 cm^{-1} of energy available for disposal into the rotational and translational degrees of freedom.[39]

In this manuscript, we report on our measurements of the Br_2 fragment rotational distributions that result from the vibrational predissociation of $NeBr_2$. Our experimental apparatus and procedures are described in Sec. II, followed by presentation of our experimental results in Sec. III. In Sec. IV, our computational studies, focusing on classical trajectory calculations are described. In Sec. V, we discuss all of these results in light of the extensive extant data and calculations on rare gas–halogen van der Waals molecules.

II. EXPERIMENT

Br_2 rotational distributions resulting from the dissociation of the $NeBr_2$ van der Waals complex were detected using a pump–probe excitation scheme. The wavelength of the pump laser is fixed to prepare $NeBr_2$ molecules in a specific vibrational level of the B electronic state using the well characterized $B \leftarrow X$ electronic transition. Following a delay of 15 ns to assure dissociation of the complex, the probe laser interrogates the fragment distribution using the $E \leftarrow B$ transitions at $\approx$305 nm. Total $E \rightarrow B$ emission was detected as a function of probe laser wavelength, yielding a excitation scan with intensities that reflect the Br_2 fragment rovibrational populations. Favorable probe transitions for particular Br_2 product vibrational levels were selected by reference to the $E \leftrightarrow B$ Franck–Condon factors calculated by Berwanger, *et al.*,[40] In all cases, the $B \leftarrow X$ transitions pumped are due to the $Ne^{79}Br_2$ complex so that the detected fragments are the homonuclear $^{79}Br_2$ molecule.

The experimental apparatus used in this investigation has been described in detail in previous reports from this laboratory.[35,41,42] Briefly, $NeBr_2$ van der Waals molecules are generated in the pulsed supersonic free jet expansion of a gas mixture composed of 20 Torr of Br_2 and a 10% Ne, 90% He carrier gas at a total pressure of 300 psig. (The Br_2 reservoir is held at -15 °C to achieve this vapor pressure.) The expansion source is a pulsed solenoid valve (General Valve) with an orifice diameter of 150 μm. Our pump laser is a Nd^{3+}-YAG pumped dye laser (Continuum Lasers YG580-30/TDL-50) operating with Rhodamine 590, Coumarin 540A, or Coumarin 500 laser dyes (Exciton) over the wavelength range 524–580 nm. The probe laser is a N_2-pumped dye laser (Laser Photonics UV24/DL14P) operating with Rhodamine 610 laser dye (Exciton). With the intracavity étalon installed, this laser typically generates pulses with an

energy of ≈300 μJ at 617 nm. Tuning of the probe dye laser wavelength is accomplished by pressure scanning with N_2 gas. The visible output of the probe dye laser is frequency doubled with KDP in an autotracking second harmonic generator (Inrad Autotracker II) and combined with the pump laser beam using a dichroic filter. The merged pump and probe laser beams intersect the supersonic free jet expansion at a right angle to the expansion axis 30 nozzle diameters from the source. In a typical experiment, the delay between the pump and probe laser pulses was fixed at 15 ns. $E \rightarrow B$ laser-induced fluorescence was collected by a $f/1.2$ optical system and detected by a UV sensitive photomultiplier tube (Thorn/EMI 9813QB). The photocathode was spatially masked to substantially eliminate Doppler broadening; scattered light from the pump laser was eliminated using a colored glass filter (Hoya Optics U-340). The output of the phototube was routed to a gated integrator (Stanford Research Systems SR250). Integrated fluorescence intensities were stored on a laboratory computer (Macintosh IIci) using LabView software (National Instruments).

As in our earlier investigation on IBr fragments from the dissociation of NeIBr,[35,42] we have demonstrated the ease with which the intense halogen valence to ion-pair electronic transitions (such as the $E \leftarrow B$ transition in Br_2) can be saturated by only moderate laser pulse energies. In these investigations, after filtering out the visible dye laser fundamental, we attenuate the ultraviolet probe laser intensity with neutral density filters to assure that the probe transition is unsaturated. Typical probe laser pulse energies were 100 nJ, though scans were recorded with pulse energies that were higher and lower to assure that the rotational distributions did not show any systematic dependence on laser pulse energy. As noted earlier, the delay between the pump and probe laser was typically fixed at 15 ns. To assure that the observed distributions were nascent, scans were also recorded with delays as long as 100 ns. No systematic dependence of the rotational distributions on this delay setting was observed. Finally, the photodissociation of chemically bound species is frequently accompanied by a substantial degree of alignment of the photofragments with respect to the polarization axis of the photolysis laser.[43] The ramification of such an effect in the present experiments would be deviations of the relative rotational line strength factors for the probe transition from those given by the traditional Höhl–London factors. To test for the presence of alignment in the dissociation of $NeBr_2$, we recorded rotationally resolved photofragment spectra while selectively detecting emission polarized parallel and perpendicular to the pump laser axis. (The probe and pump lasers are polarized perpendicular with respect to one another.) No systematic dependence of the spectra on the polarization of the detected emission was noted. We assume, therefore, that alignment of the Br_2 fragment is negligible.

III. EXPERIMENTAL RESULTS

In Fig. 1, we display a typical $E \leftarrow B$ fluorescence excitation scan of the $v=14$ Br_2 fragments that result from the dissociation of $v=15$ $NeBr_2$, along with our best fit to the spectrum. The rotational populations that are derived from these data are displayed in Fig. 2. The error bars shown in Fig. 2 reflect the distribution of populations for a particular rotational level derived from different data sets. The uncertainties are significantly larger for the lower j levels because extraction of populations in the bandhead region is highly susceptible to relatively small levels of noise in our spectra.

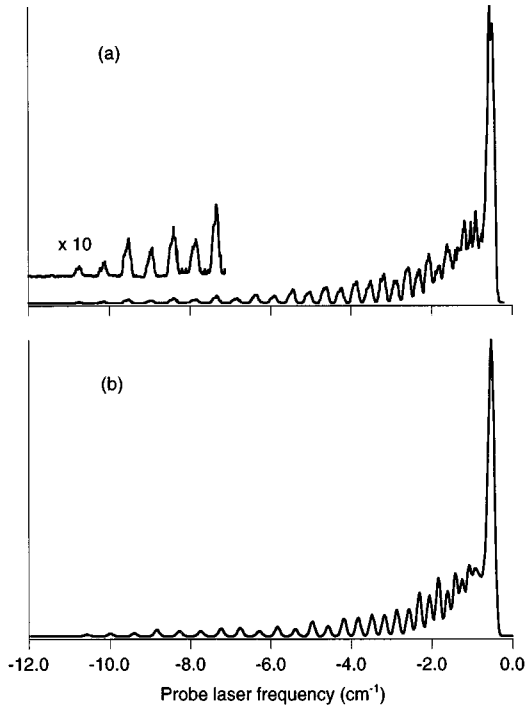

FIG. 1. (1,14) $E \leftarrow B$ fluorescence excitation scan of Br_2 fragments from the dissociation of $NeBr_2$ prepared in the $v=15$ level of the B electronic state. (a) Experimental data; (b) simulated spectrum using rotational state populations derived from a least-squares fit to the experimental data.

In Fig. 1(a) an intensity alternation in features originating from even and odd Br_2 rotational states in the B electronic state is clearly seen. In their studies of the dissociation of the $NeCl_2$ and $HeCl_2$ molecules, Cline *et al.* observed that the Cl_2 fragments obeyed parity conservation due to the symmetry of the van der Waals potential (and the homonuclear character of the diatomic halogen).[26,28] Excitation of complexes to single rotational levels with $(+)$ parity generated Cl_2 fragments with only even values of the rotational quantum number, j, while complexes with $(-)$ parity generated fragments with only odd values of j.[26,28] In $NeBr_2$, the same effect is operable, with the thermal distribution of population among the rotational levels of the complex and the nuclear spin statistics generating a mixture of $(+)$ and $(-)$ parity rotational levels in the ground electronic state. In addition, the homogeneous broadening of the $B \leftarrow X$ excitation features and the ≈0.25 cm^{-1} bandwidth of our pump laser conspire to make excitation of a single B state rotational level impossible. Thus our pump laser prepares complexes with an indeterminant mixture of $(+)$ and $(-)$ parity, which generates a mixture of even and odd j fragment rotational levels. This mixture will vary with the $NeBr_2$ vibrational state popu-

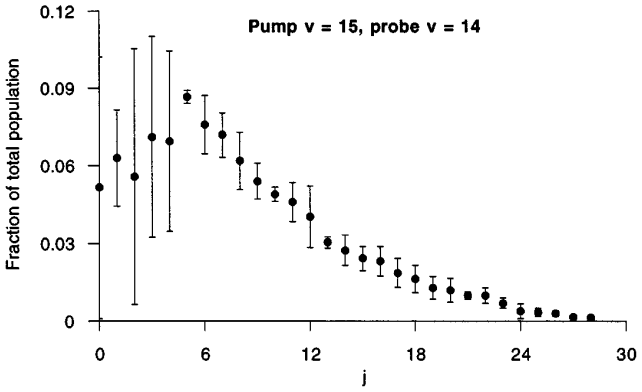

FIG. 2. Distributions of rotational states in $v=14$ following the $\Delta v=-1$ dissociation of $v=15$ $NeBr_2$. The distribution is normalized such that the sum of the populations equals one.

lated as the underlying rotational structure due to the complex changes with the vibrationally averaged Br_2 bondlength. To simplify the display of these distributions and to facilitate comparisons between $NeBr_2$ vibrational levels, we have separately normalized the even and odd j distributions and plotted them on a single axis system as shown in Fig. 2. This has the effect of presenting all of our distributions as if our pump laser prepared equal numbers of $(+)$ and $(-)$ rotational levels.

In Fig. 3, we present the Br_2 fragment rotational distributions that arise from $NeBr_2$ following excitation to several additional B electronic state vibrational levels. In each case the fragments are produced after the loss of one quantum of vibrational energy (a $\Delta v=-1$ process). In Fig. 3(a) the rotational distribution for the $v=10\rightarrow v=9$ dissociation channel is shown along with the $T=6.9$ K Boltzmann distribution derived by Sivakumar *et al.* for the same process.[39] Considering the severe constraints imposed by the form of a Boltzmann distribution, the agreement with our higher resolution data is excellent.

Cline *et al.* measured the fragment vibrational state distribution that results from the dissociation of $NeBr_2$ and observed that $v=27$ is the highest vibrational level for which $\Delta v=-1$ fragmentation products are observed.[38] Assuming that the energetics of the dissociation provide the dominant constraint leading to this observation, these authors were able to derive a binding energy of 62 ± 2 cm^{-1} for $NeBr_2$ in the B electronic state, $v=27$, and 70 ± 2 cm^{-1} for the X state, $v=0$.[38] In Fig. 3(f), we note that following dissociation of $v=27$ $NeBr_2$, the rotational distribution in $v=26$ fragments terminates at $j=7$. (Note that our least-squares fitting routine assigns small populations to $j=8$ and 9, but that the error bars make these values experimentally insignificant.) We interpret the termination of this distribution as reaching the energetic limit for dissociation of the complex with loss of one quantum of vibrational excitation. Using the known rotational constants for $^{79}Br_2$,[44] we can, therefore, further bracket the dissociation energy for the B state, $v=27$, as $60.57\leqslant D_0\leqslant 61.22$ cm^{-1}, or $D_0=60.90\pm0.33$ cm^{-1}, in agreement with the lower resolution result of Cline *et al.*[38]

Based on a model presented first by Cline *et al.* for $NeCl_2$,[28] we have previously detailed the corrections that must be made to binding energies derived from the termination of fragment rotational distributions.[35] Briefly, the analysis presented above assumes that the dominant energetic constraint on the population of fragment rotational energies is the asymptotic energies (i.e., the energies at large $Ne-Br_2$ separations) of the Br_2 rotational levels. In fact, rotational excitation of the fragments implies a degree of orbital angular momentum in the complex and a resulting centrifugal barrier in the van der Waals potential. Cline *et al.* proposed a procedure for estimating the magnitude of the centrifugal barrier and the correction factor required to adjust the derived binding energy.[28] In the interest of brevity we omit a detailed discussion, but once the centrifugal barrier is estimated, the revised B state, $v=27$ binding energy is $60.12\leqslant D_0\leqslant 60.91$ cm^{-1}. An additional uncertainty in the derivation of the binding energies is the degree of rotational excitation in the $NeBr_2$ complex prior to dissociation. Under our experimental conditions, we have found the rotational temperature to be 0.9 K, suggesting that more that 90% of the complexes have less than 1.4 cm^{-1} of rotational energy. The presence of rotational excitation has the effect of underestimating the true value of D_0 by up to 1.4 cm^{-1}. We incorporate this possibility into our calculation by extending the range of possible dissociation energies by this amount. Our final estimate is then $60.1\leqslant D_0\leqslant 62.3$ cm^{-1} or $D_0=61.2\pm1.1$ cm^{-1} for the B state, $v=27$. From the band shift of the $NeBr_2$ $B\leftarrow X$ excitation features relative to those of uncomplexed Br_2,[36] we can calculate the X state, $v=0$ dissociation energy and the dissociation energy for other B state vibrational levels. The B state values are presented in Table I; the X state, $v=0$ dissociation energy is found to be $D_0=70.0\pm1.1$ cm^{-1}.

Table I summarizes the energetic data for the dissociation pathways that we have examined. The energy available for disposal into the rotational and translational degrees of freedom in the fragments (E_{avl}) is shown, along with the average fragment rotational energy, $\langle E_{\mathrm{rot}}\rangle$, calculated from the observed rotational distributions. $j_{\max}$ is the highest rotational level *observed* with statistically significant population. j_{avl} is the highest rotational level that is *available* to be populated given the available energy and the estimated height of the centrifugal barrier. Note that in most cases, the measured rotational distributions extend to approximately the maximum value of j consistent with the maximum available energy. Indeed, given the limitations on the accuracy of our model for the centrifugal barrier (particularly for higher values of j), we consider it likely that all of the rotational distributions for $\Delta v=-1$ fragmentation pathways extend to their effective energetic limits.

The fragment energetic information in Table I can be directly compared to the rotational infinite order sudden approximation calculations of Buchachenko *et al.*[15] Using a variety of model potential energy surfaces, these investigators calculate values of $\langle E_{\mathrm{rot}}\rangle$ that are substantially smaller than those revealed in our experiments. The variation of the cal-

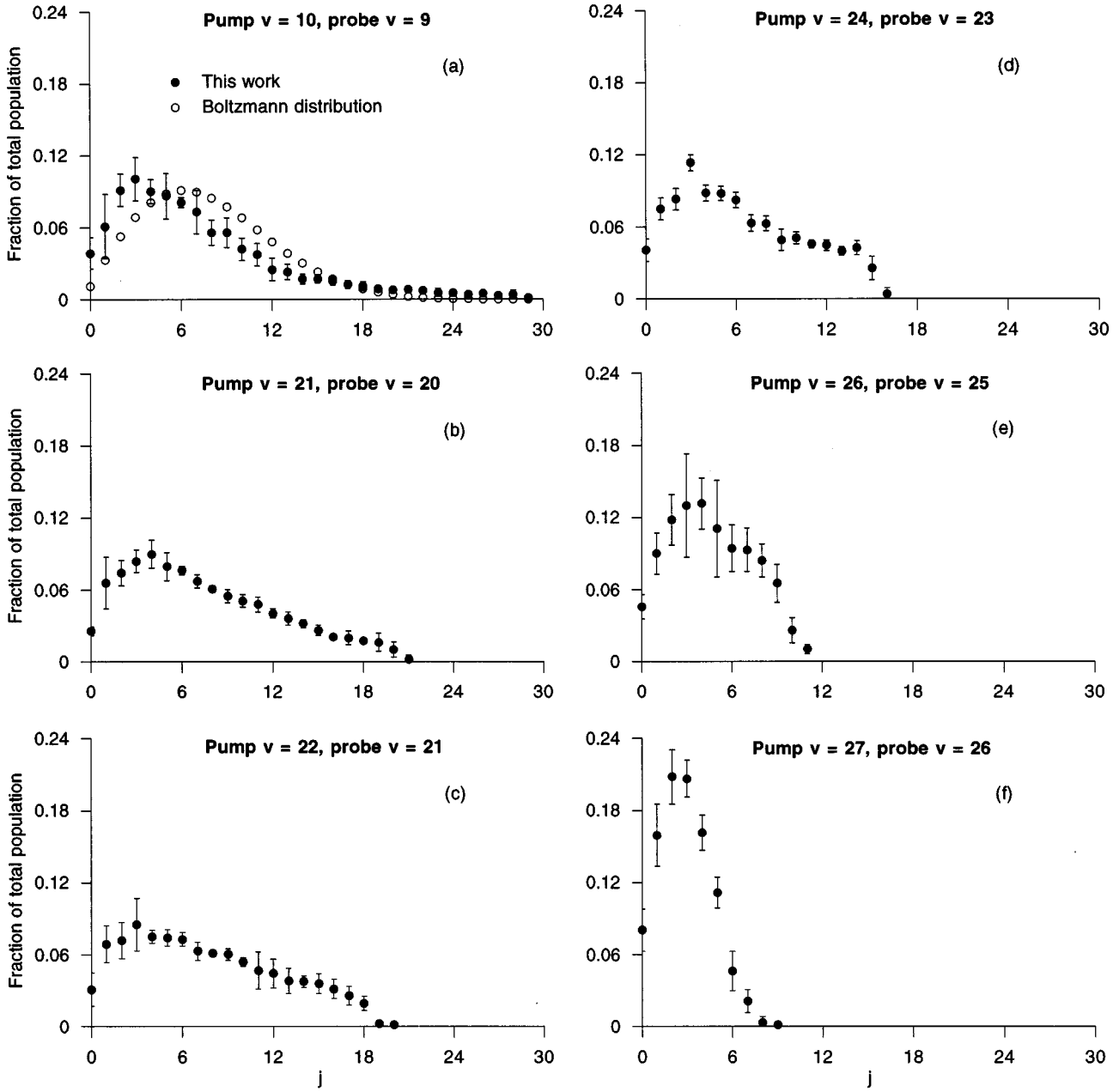

FIG. 3. Distributions of rotational states resulting from $\Delta v=-1$ dissociation events in $NeBr_2$. Each distribution is normalized such that the sum of the populations equals one. (a) $v=10\rightarrow v=9$. The Boltzmann distribution is that derived in Ref. 39; (b) $v=21\rightarrow v=20$; (c) $v=22\rightarrow v=21$; (d) $v=24\rightarrow v=23$; (e) $v=26\rightarrow v=25$; (f) $v=27\rightarrow v=26$.

culated values of $\langle E_{\mathrm{rot}}\rangle$ with B state vibrational level does, however, mimic the experimental data.[15]

In Fig. 4, we have plotted several of the rotational distributions that result from $\Delta v=-1$ dissociation events on the same axis system. Note that the horizontal axis is rotational energy, not rotational quantum number, so that the effects of varying rotational constants with Br_2 vibrational state are eliminated. (We have omitted the error bars on this figure for clarity.) Aside from different values of $j_{\max}$, these distributions are the same within experimental error. This insensitivity of the form of the rotational distribution to E_{avl} (aside from the position of the energetic cutoff) is reminiscent of the behavior observed for $NeCl_2$,[28] but is quite different from that observed in NeICl.[24]

In Fig. 5, rotational distributions that arise when $NeBr_2$ dissociates with the loss of two quanta of vibrational excitation ($\Delta v=-2$ processes) are displayed. In general, we find that the distributions extend to much higher rotational levels, and that the fraction of the available energy that appears in fragment rotational excitation is intermediate to the extreme values observed for $\Delta v=-1$ processes (Table I). A detailed comparison of Table I reveals, however, that for dissociation events with similar values of E_{avl} ($v=10\rightarrow v=9$ and $v=27\rightarrow v=25$, for example, or $v=15\rightarrow v=14$ and

TABLE I. $NeBr_2$ predissociation energetics.

Initial v	D_0 (cm^{-1})	Final v	E_{avl} (cm^{-1})	$\langle E_{rot}\rangle$ (cm^{-1})	$\langle E_{rot}\rangle/E_{avl}$	j_{avl}	j_{max}
$\Delta v=-1$							
10	64.3	9	67.7	5.1	0.075	29	29
15	63.6	14	48.7	5.4	0.11	26	28
21	62.0	20	25.6	4.1	0.16	20	20
22	62.5	21	21.0	4.0	0.19	18	18
24	62.4	23	12.9	2.8	0.22	15	15
26	62.0	25	5.4	1.4	0.26	10	11
27	61.2	26	2.3	0.6	0.26	8	7
$\Delta v=-2$							
24	62.4	22	92.3	8.1	0.088	35	34
26	62.0	24	76.7	11.4	0.15	33	38
27	61.8	25	69.6	9.0	0.13	32	36
29	60.4	27	55.3	8.5	0.15	29	33

$v=29\rightarrow v=27$), the $\Delta v=-2$ pathways result in significantly higher fractions of the total available energy being channeled into fragment rotational excitation. As in the case of $\Delta v=-1$ pathways, we observe population in rotational levels that are substantially at the energetic limit for rotational excitation. Note that the high values of rotational quantum number accessed make our simple model for the centrifugal barrier used in our calculation of j_{avl} particularly suspect, such that discrepancies between j_{avl} and j_{max} (Table I) are not considered significant.

IV. COMPUTATIONAL MODELS FOR FRAGMENT ROTATIONAL EXCITATION

In our previous report on the IBr rotational distributions that result from the dissociation of NeIBr, we used three approximate computational models to explore the qualitative origin of the IBr rotational excitation.[35] In our current investigation of $NeBr_2$, we have applied these same models to an investigation of the Br_2 rotational distributions. While none of these models provides the accuracy of quantum dynamics simulations, they do allow us to explore the essential forces that govern the disposal of energy in the vibrational predissociation process. In the sections that follow, we briefly review the implementation of these models; for more complete details, the reader is referred to our previous work on NeIBr.[35]

Each of these calculations requires a model potential energy surface for $NeBr_2$ and our model surface is displayed in Fig. 6. To construct this surface, we assume that the Ne–Br_2 interaction potential energy at a particular point in space can be written as a sum of two Ne–Br interactions. The individual atom–atom interactions are modeled as Morse potentials; the potential parameters are $D_e=42.0$ cm^{-1}, $\alpha=1.67$ $Å^{-1}$, $r_{av}=3.90$ Å, and are the same as those used to describe the Ne–Br interaction in NeIBr.[42] As a sum of atom–atom Morse potentials, this surface lacks the proper $1/R^6$ functional form for large Ne–Br_2 distances. Given the approximate nature of the models that we implement in this work, however, we believe that this form is adequate to extract the *qualitative* information that we seek regarding the disposal of energy in the vibrational predissociation. Surfaces of this form have been used with considerable success in simulations of the dynamics of HeI_2,[12] HeICl,[8] and NeICl.[13] In addition, quantum wave packet calculations carried out on $HeCl_2$ and $NeCl_2$ show little sensitivity to the addition of a long range $1/R^6$ tail to additive atom–atom potentials.[9]

A more serious uncertainty regarding the $NeBr_2$ potential energy surface arises in the context of several recent investigations that point to the importance of energy minima in linear configurations for rare gas–Cl_2 and ClF van der Waals complexes.[16,45–49] In $HeCl_2$, for example, multiple minima on the ground electronic state potential surface are found to be essential to obtain an adequate theoretical fit to experimental spectroscopic and scattering data.[16] In the excited B electronic states, however, the consensus view is that the minima in the T-shaped geometry are adequate to reproduce both the dynamics and spectroscopic measurements;[16,50] the potential surface adopted for our $NeBr_2$ studies is in accord with this result.

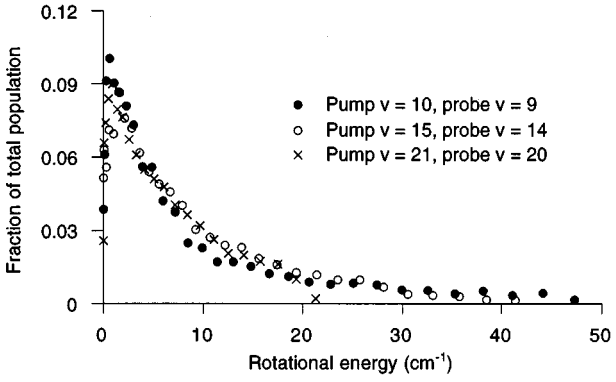

FIG. 4. Distributions of rotational states for three $\Delta v=-1$ dissociation events in $NeBr_2$. The horizontal axis is rotational energy, not rotational quantum number, to facilitate comparison of distributions with different rotational constants.

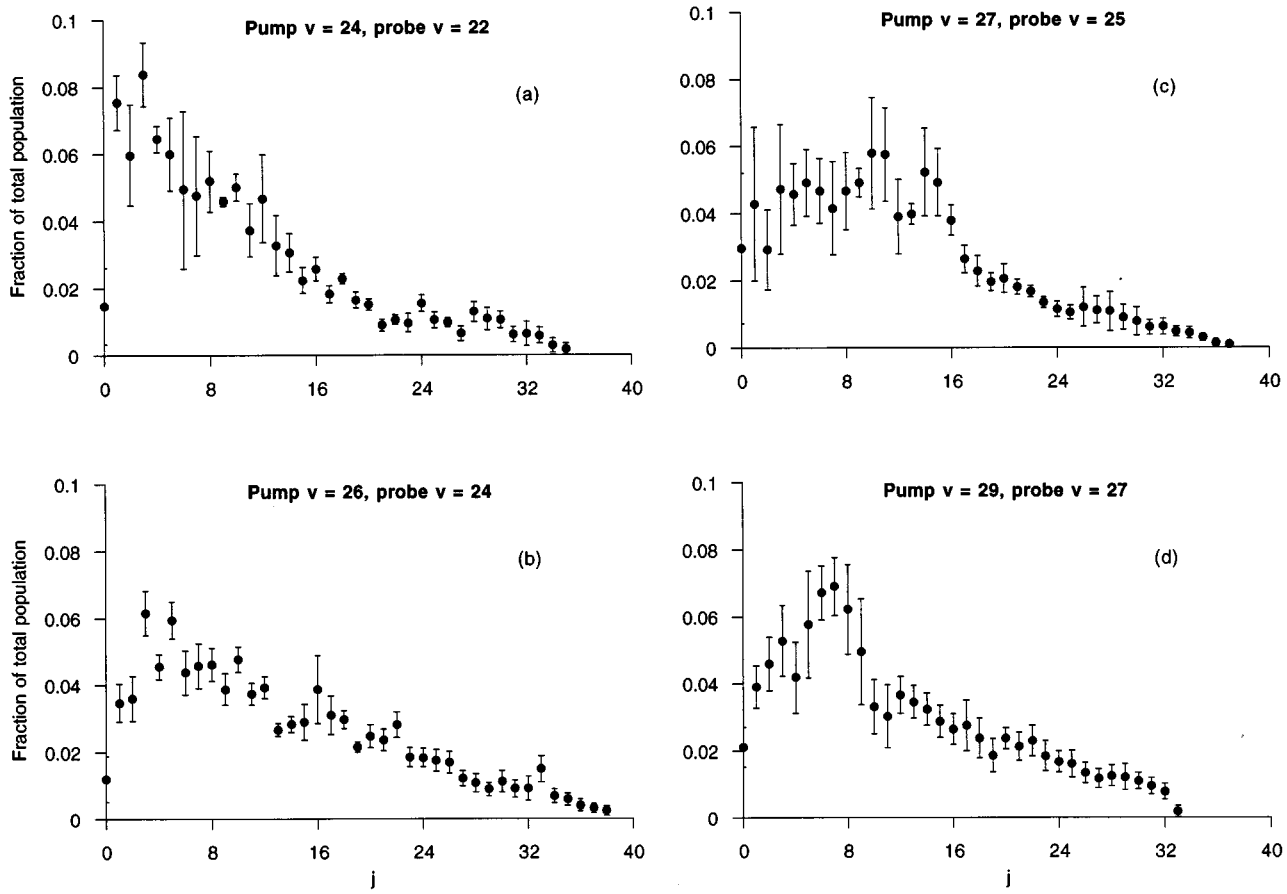

FIG. 5. Distributions of rotational states resulting from $\Delta v=-2$ dissociation events in $NeBr_2$. Each distribution is normalized such that the sum of the populations equals one. (a) $v=24\rightarrow v=22$; (b) $v=26\rightarrow v=24$; (c) $v=27\rightarrow v=25$; (d) $v=29\rightarrow v=27$.

A. Bound state calculation and the Franck–Condon model

As in our previous study of NeIBr,[35] we have applied the quantum mechanical bound state programs of Halberstadt and co-workers[7,8,11,13,51] to the $NeBr_2$ system using our model potential energy surface. This calculations are based on the methodology described in considerable detail elsewhere by Halberstadt, Beswick, and co-workers.[7,8,11,13,51]

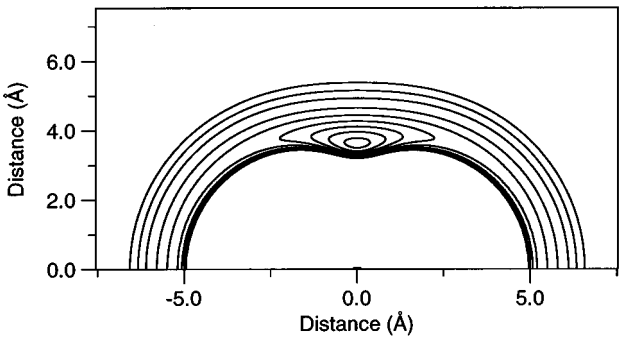

FIG. 6. Model potential energy surface for $NeBr_2$. The origin of the coordinate system is fixed at the center of mass of Br_2. The energy contours are drawn at 10 cm^{-1} intervals, with the outermost contour lying -10 cm^{-1} relative to the energy of separated $Ne+Br_2$.

Briefly, the Hamiltonian operator is written in terms of the internal coordinates r, the magnitude of the vector from one Br atom to the other, R, the magnitude of the position vector of the Ne atom relative to the Br_2 center of mass and γ, the angle between these two vectors. The higher frequency Br_2 vibrational motion is separated from the lower frequency van der Waals vibrational motion by calculating the bound state energies and wave functions for an effective $Ne–Br_2$ potential in which our model potential $V(r,R,\gamma)$ is averaged over the Br_2 vibrational motion. Using this approximation, the averaged Hamiltonian $H_{v,v}$ for the $NeBr_2$ complex that correlates with Br_2 vibrational level v is written as[7,8,11,13,51]

$$H_{v,v}=-\frac{\hbar^2}{2\mu}\frac{\partial^2}{\partial R^2}+\frac{l^2}{2\mu R^2}+V_{v,v}(R,\gamma)$$

$$+E_{\mathrm{Br}}(v)+\frac{B_v}{\hbar^2}j^2.$$

$V_{v,v}(R,\gamma)$ is the averaged intermolecular van der Waals potential, while $E_{\mathrm{Br}}(v)$ is the vibrational eigenvalue for uncomplexed Br_2. B_v is the relevant Br_2 rotational constant and μ is the reduced mass of the $Ne–Br_2$ system. For these calculations we fix the total angular momentum, J, to 0.

The desired wave functions, $\psi_{k,v}(R,\gamma)$ which describe the motion of the Ne atom relative to Br_2, are the eigenfunc-

tions of $H_{v,v}$. This Hamiltonian is diagonalized using a finite two dimensional (R,γ) basis set, with each basis set function written as a product of an angular and a radial function. The radial functions are harmonic oscillator functions, while the angular functions are obtained by prediagonalization of the angular part of $H_{v,v}$ using a basis set of Br_2 free rotor functions at a specified $R=R_e=3.65$ Å. For $J=0$, these functions are simply appropriately normalized spherical harmonics, $Y_{j,0}(\gamma)$. The detailed composition of the basis functions is described in Refs. 7, 8, 13, and 51. In our calculations, we use 15 harmonic oscillator functions to describe the R-dependence of the Ne wave function along with 15 bending basis functions, each composed of 30 Br_2 free rotor functions with even values of the quantum number j. (Because of the symmetry of the potential, when total angular momentum, J, is 0, only even j fragment rotational states have the appropriate parity characteristics.)

As a preliminary test of the model van der Waals potential energy surface, we consider the predicted dissociation energy D_0. The calculated value is found to be 64.0 cm^{-1} for the B state, $v=10$, a value that is in exact agreement with the experimentally determined figure of 64.3 ± 1.1 cm^{-1}. We conclude from this result that the shape and depth of the potential well on our model potential energy surface are at least qualitatively correct.

In the Franck–Condon model for the dissociation of $NeBr_2$, rotational excitation of the Br_2 fragments arises from the zero-point bending motion that is initially prepared prior to dissociation.[1,52] Application of the Franck–Condon model in this case is particularly facile because in the bound state calculation we represent the wave function of the quasibound Ne atom in terms of the Br_2 free rotor basis set. In Fig. 7(a), we present the result of applying such a model to the dissociation of $NeBr_2$ from the B electronic state, $v=10$. Note that the restriction of our calculations to $J=0$ requires that only the even values of j are populated in the dissociation.

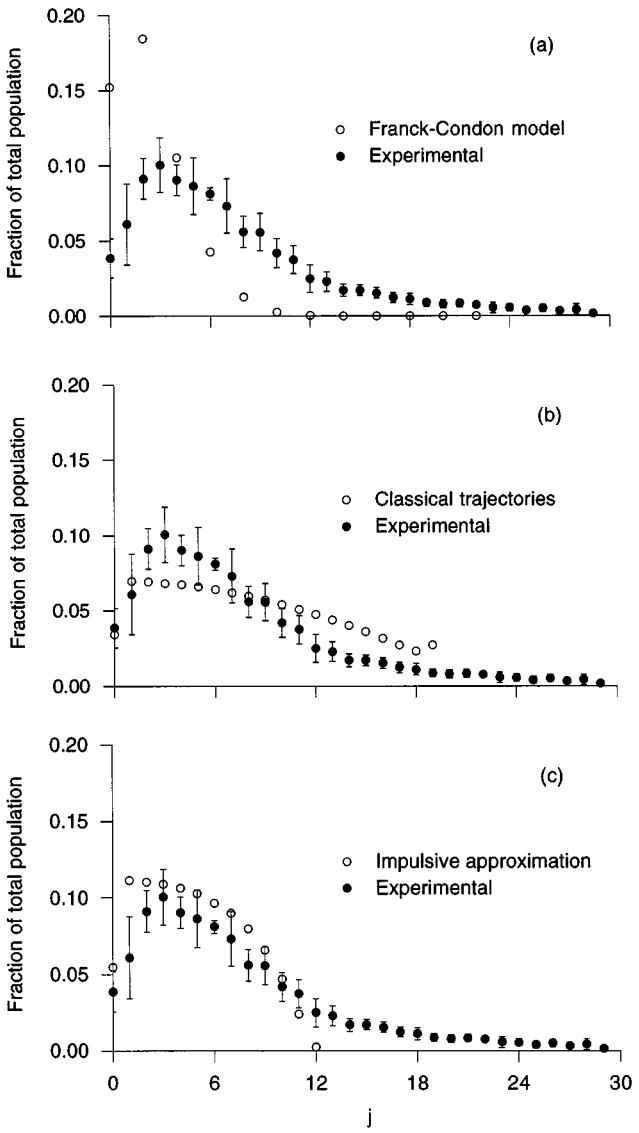

FIG. 7. Theoretical models for Br_2 fragment rotational excitation (open circles) compared with the experimental data (solid circles) for the $\Delta v=-1$ dissociation of $v=10$ $NeBr_2$. (a) Franck–Condon model; (b) classical trajectory model; (c) classical impulsive approximation.

B. Semiclassical model for vibrational predissociation

In our previous investigation of NeIBr,[35] we adopted the semiclassical model for the dissociation of rare gas–halogen van der Waals molecules developed by Waterland *et al.*[25] In this approach, Waterland *et al.* assumed that the van der Waals complex is transferred from the initially prepared quasi-bound level correlating with the halogen vibrational level v to the repulsive wall of the van der Waals potential correlating with vibrational level $v-1$. This transfer is assumed to occur instantaneously and without any specification of the dynamics of the intramolecular vibrational coupling mechanism. The angular position γ of the rare gas atom is conserved upon transfer to the repulsive surface; we label this initial angle γ_0. The fragment rotational distribution then arises from the scattering, at energy E_{avl}, from the repulsive wall of the $v-1$ van der Waals potential. As in our earlier investigation we have employed two models to represent the scattering process.[35] Common to both is the calculation of the classical excitation function $j(\gamma_0)$, which expresses the final fragment rotational angular momentum, j, as a function of the initial scattering angle. Waterland *et al.*[25] use the excitation function to calculate fragment rotational distributions by drawing on analogous studies by Schinke on the photodissociation of chemically bound molecules.[1,53] A central feature of this approach is the recognition that the range of fragment rotational states that can be populated is given directly by the excitation function, modulated by a weighting factor that accounts for the fact that not all initial angles γ_0 are equally probable. In the present calculations, the weighting factor is the bound state probability distribution determined in our quantum mechanical calculation (evaluated at the equilibrium van der Waals bond length, R_e). Complete mathematical details of this approach can be found in our earlier publication[35] or those of Waterland *et al.*[25] or Schinke.[1,53]

C. Classical trajectory calculations

Within the semiclassical model, the most rigorous method for calculation of the excitation function is to propagate exact classical trajectories on the model potential energy surface. In these calculations and in our analysis, we follow closely the previous work of Schinke[1,53] and Waterland *et al.*[25] Briefly, we choose the initial linear and angular momentum of the fragment to be zero. The energy of the trajectory is set to E_{avl}. For a particular choice of initial angle γ_0, the corresponding value of the radial distance R_0 is found from the condition

$$V_{\mathrm{vdw}}(R_0,\gamma_0)=E_{\mathrm{avl}},$$

such that the Ne atom is motionless on the repulsive wall of the van der Waals potential at the initiation of each trajectory. The total angular momentum, J, is set to 0 so that any fragment diatomic rotational angular momentum is exactly counter-balanced by orbital motion of the recoiling fragments. γ_0 values are chosen to lie on a uniform grid between 0 and $\pi/2$. (Because of the C_{2v} symmetry of the potential, the excitation function for γ_0 values between $\pi/2$ and π is identical to that for $0\leqslant\gamma_0\leqslant\pi/2$.) We integrate Hamilton's equations of motion for a total of 50 picoseconds for each trajectory, which is found to be sufficient for $j(t)$ to reach its asymptotic value. The resulting classical excitation function for the $v=10\rightarrow v=9$ predissociation of $NeBr_2$ is shown in Fig. 8(a), in which we have included only the most relevant angular range. Also plotted in Fig. 8(a) is the Ne atom angular probability distribution, as determined from the bound state calculation. The fragment rotational distribution that arises from this calculation is shown in Fig. 7(b) along with the experimentally measured distribution.

In our computations on the predissociation of NeIBr, we noted that the range of values of E_{avl} that are amenable to this approach are limited, at low energies, by the appearance of ''orbiting resonance'' structures in the classical dynamics.[35] This phenomenon also occurs in our $NeBr_2$ calculations, as displayed in Figs. 9 and 10. In Fig. 9, we show portions of the excitation function that correspond to the $v=21\rightarrow v=20$ predissociation of $NeBr_2$, with $E_{\mathrm{avl}}=25.6$ cm^{-1}. Note that the excitation function is no longer a smooth function of the initial angle γ_0 and that the asymptotic value of j is extraordinarily sensitive to the initial conditions. In Fig. 9(a) a relatively wide range of initial angles are displayed. Note that as compared to Fig. 8(a), the region of maximum $|j|$ has been replaced by a smooth region of significantly lower $|j|$, separated from the more conventional portion of the excitation function by regions of fluctuating values of the asymptotic angular momentum. In Fig. 9(b) we focus on one of these narrow transition regions, emphasizing that ''smooth'' regions of the excitation function are imbedded in the irregular structure. In fact, as we focus on progressively narrower regions of the irregular structure, we always find imbedded smooth structure similar to that displayed in Fig. 9(b). This form of the excitation function is thus analogous to the fractal pattern identified by Noid *et al.* in their classical studies of vibrational energy transfer in collisions of He with I_2.[54]

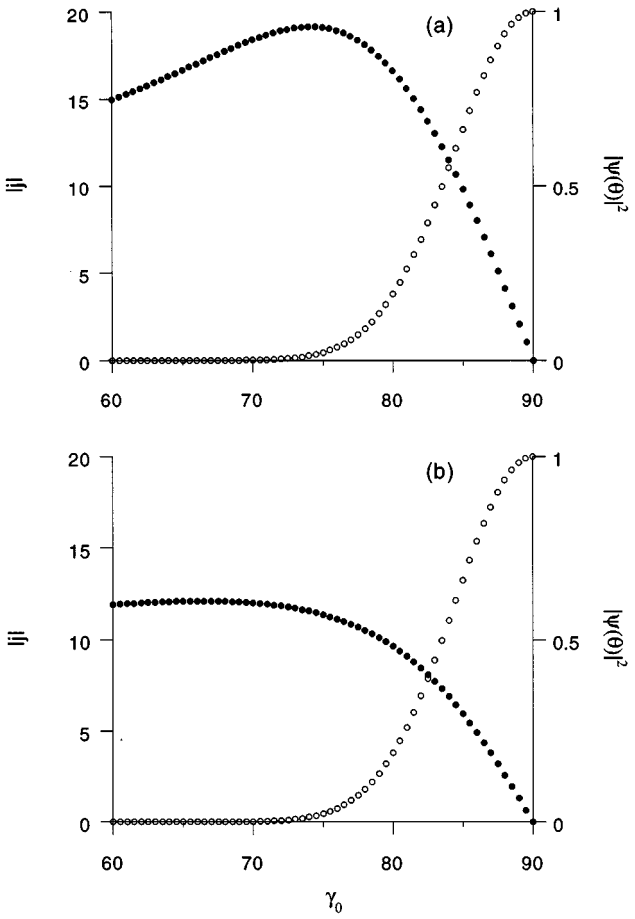

FIG. 8. Classical excitation functions (solid circles) and Ne atom angular probability distributions (open circles) used in two classical models for the dissociation of $NeBr_2$. The initial Ne–Br_2 angle γ_0 is plotted in degrees. The magnitude of the angular momentum, $|j|$, is plotted in units of $\hbar$. The probability distributions are normalized such that the maximum value is 1.0. (a) Classical trajectory calculations; (b) classical impulsive calculations.

In Fig. 10, we display a plot of $|j|$ vs time for two of the trajectories selected from the excitation function of Fig. 9. In Fig. 10(a), a trajectory that is typical of the ''conventional'' regions of the excitation function ($\gamma_0=82.0°$) is shown. In Fig. 10(b), in contrast, one of the trajectories that gives rise to an ''unconventional'' point ($\gamma_0=80.2°$) is selected. From these plots and a detailed examination of the energetics of the trajectories, the origin of the structure in the excitation function is clear. When $\gamma_0=80.2°$, early in the trajectory the Ne atom passes through a region of potential anisotropy, resulting in considerable Br_2 rotational angular momentum and orbital angular momentum of the separating fragments. (Recall that since the total angular momentum, J, is 0, the orbital angular momentum of the Ne atom must be balanced by the rotational angular momentum of the Br_2 fragment.) Specifically we observe that the sum of the rotational energy of the fragments and the centrifugal energy associated with the orbital motion exceed E_{avl}. Thus the fragments are ''trapped'' in the attractive portion of the potential energy

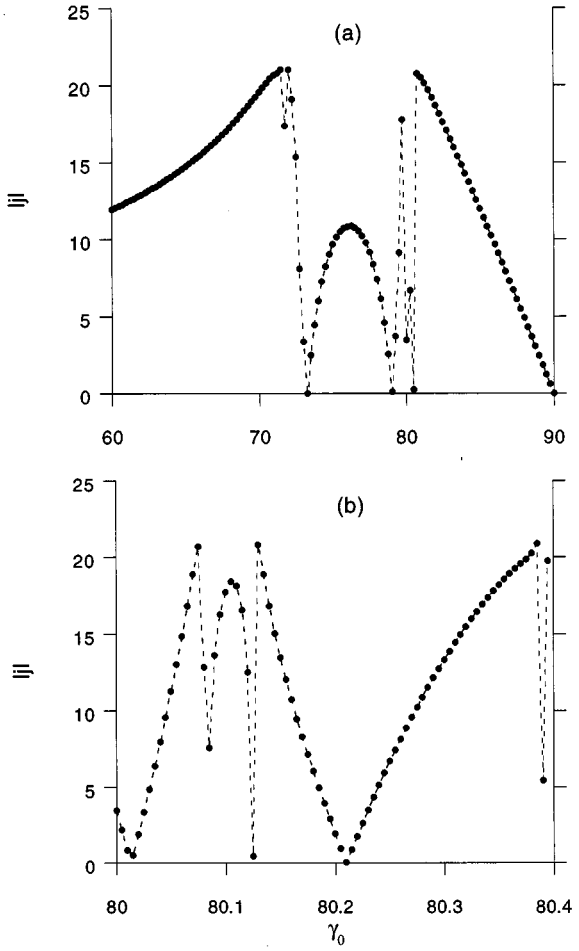

FIG. 9. Classical excitation functions from classical trajectory calculations at a low value of available energy (E_{avl}=25.6 cm^{-1}). The initial Ne–Br_2 angle, γ_0, is plotted in degrees. The magnitude of the angular momentum, $|j|$, is plotted in units of $\hbar$. (a) $60° \leqslant \gamma_0 \leqslant 90°$; (b) $80.0° \leqslant \gamma_0 \leqslant 80.4°$.

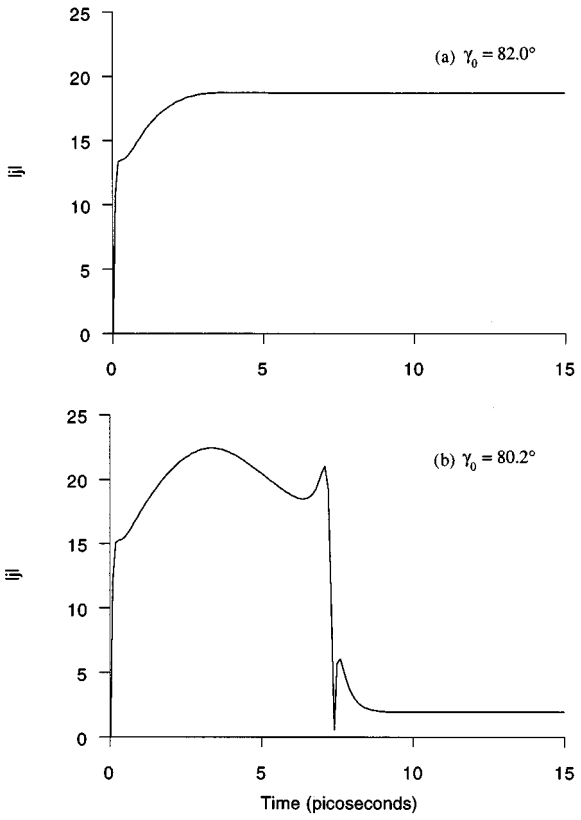

FIG. 10. Temporal evolution of the angular momentum for two of initial conditions displayed in Fig. 9. The magnitude of the angular momentum, $|j|$, is plotted in units of $\hbar$. (a) γ_0=82.0°; (b) γ_0=80.2°.

surface. For the trajectory shown in Fig. 10(b), the rotational and centrifugal energies sum to 32.4 cm^{-1} at t=3.3 ps, while the E_{avl}=25.6 cm^{-1}. A second encounter with the repulsive wall (at 7.4 ps when γ_0=80.2°) is required to quench the fragment angular momentum and allow the eventual dissociation. It is apparent from the structure in the excitation function that the trapping phenomenon and the eventual magnitude of the angular momentum quenching are extraordinarily sensitive to the initial conditions selected for the trajectory. An interesting further investigation would be to examine the quantum dynamics in this energy regime to reveal the presence or absence of quantum mechanical manifestations of this result.

D. Classical impulsive approximation

As a test of the importance of final state interactions induced by the full potential energy surface in determining the fragment quantum state distribution, we have also calculated the excitation function $j(\gamma_0)$ as if the interaction were entirely impulsive in nature. In this calculation we simplify the potential by including only the repulsive wall at an energy of E_{avl} and considering the scattering of the Ne atom from this contour. In this situation, the Br_2 attains its final rotational angular momentum instantaneously and we determine this value from the expression[25]

$$j^2 = \frac{E_{avl}}{B_v + 1/(2\mu b^2)},$$

by calculating the effective impact parameter (b) associated with each initial atomic configuration. In Fig. 8(b), the classical excitation function that we obtain from this model for rotational excitation is presented. The rotational distribution predicted using this model is shown in Fig. 7(c) along with the experimental data.

V. DISCUSSION

The Franck–Condon model for the dissociation of rare gas–halogen van der Waals complexes has consistently failed to reproduce the breadth of fragment rotational distributions in Cl_2–, ICl-, and IBr-containing molecules.[8,28,35] As documented in Fig. 7(a), the results that we report here on Br_2 fragments from the dissociation of $NeBr_2$ are no exception. Cline *et al.* noted that in the case of $NeCl_2$, however, the Franck–Condon model is representative of certain features of the data, specifically the insensitivity of the rotational distributions to the value of E_{avl}.[28] The width of the Franck–Condon predicted rotational distribution is inversely related to the breath of the zero-point bending wave function,

with the later parameter determined by the angular anisotropy of the van der Waals potential energy surface and the atomic masses. The value of E_{avl} and the actual postion of the potential minima relative to the diatomic fragment internuclear axis are irrelevant in this model for the dissociation. As we have noted previously and display in Fig. 4, for Br_2 fragments from $NeBr_2$ we also observe an insensitivity of the fragment rotational distributions to the value of E_{avl}. The Franck–Condon model also predicts that the $\Delta v=-2$ dissociation pathways should lead to the same fragment rotational distributions as the $\Delta v=-1$ pathways. This behavior was observed in $NeCl_2$, with the conclusion that the $\Delta v=-2$ dissociation products arose from a direct coupling from the quasi-bound state correlating with vibrational level v to continuum levels correlating with vibrational level $v-2$.[28] As the data in Table I indicates, however, $\Delta v=-2$ dissociation events in $NeBr_2$ channel substantially more energy into rotational energy than $\Delta v=-1$ dissociation events (for dissociation pathways with comparable E_{avl}). This behavior suggests a different mechanism for the $\Delta v=-2$ events in $NeBr_2$. In $ArCl_2$, experiments and calculations have implicated stepwise intramolecular vibrational redistribution in the dissociation dynamics.[6,10,17,30] In this scheme, the quasibound state correlating with vibrational v is coupled most strongly with a small number of also quasibound states correlating with vibrational level $v-1$. The latter levels are then coupled directly to the continuum to generate $\Delta v=-2$ fragments via an indirect mechanism. It would be interesting to discover whether similar mechanisms are operative in complexes such as $NeBr_2$ and to explore the origin of the differences with the lighter $NeCl_2$.

We demonstrate the importance of the full anisotropy of the van der Waals potential energy surface in models of the dissociation dynamics in Figs. 7(b) and 7(c). From the comparison shown in Fig. 7(c), it is clear that modeling the dissociation as a simple impulsive half-collision with the repulsive wall of the potential is a dramatic oversimplification. This result is not surprising, given that the available energy is comparable in magnitude to the depth of the potential well. We expect, therefore, that the dynamics will be strongly affected by the anisotropy of the full potential.

Figure 7(b) shows that the classical trajectory approach is superior to the other models considered here for the dissociation of $NeBr_2$, but that it falls far short of reproducing the population in the highest rotational levels. On the other hand, it predicts an average rotational energy, $\langle E_{rot}\rangle$, of 5.5 cm^{-1}, a value that is somewhat higher than that observed experimentally (see Table I; $\langle E_{rot}\rangle=5.1$ cm^{-1}). In contrast to these data, when we applied the semiclassical model to the dissociation of NeIBr, the calculated distribution extended to the same rotational level as the experimental data, though the calculated value of $\langle E_{rot}\rangle$ (4.6 cm^{-1}) remained somewhat larger than the experimental value (3.9 cm^{-1}).[35] Our central concern in the remainder of this section is to address the differences in the agreement of the calculated and experimental results for NeIBr and $NeBr_2$ and to suggest regimes in which the classical trajectory approach might be more or less appropriate.

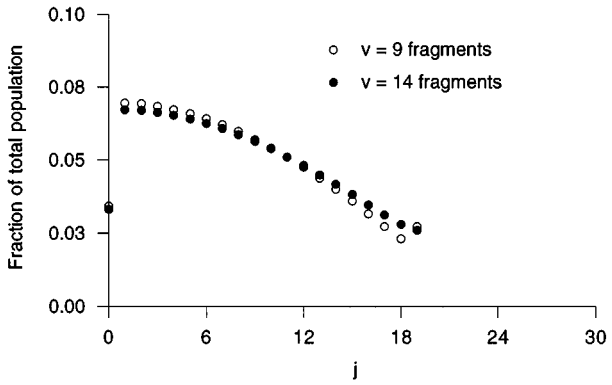

FIG. 11. Rotational distributions predicted by the classical trajectory model for the $v=15\rightarrow v=14$ ($E_{avl}=67.7$ cm^{-1}) and $v=10\rightarrow v=9$ ($E_{avl}=48.7$ cm^{-1}) dissociation events. Each distribution is normalized such that the sum of the populations equals one.

One test of the classical trajectory approach is to explore the variation of the calculated distributions with the various dissociation channels. In Fig. 11, we present a comparison of the calculated rotational distributions for the $v=9$ and $v=14$ Br_2 fragments that result from $\Delta v=-1$ dissociation pathways. The surprising result is that the calculated distributions are nearly identical. This behavior mimics the experimental data (Fig. 4) in which the only significant difference in the $v=9$ and $v=14$ distributions is the value of j_{max}. As noted previously, Cline *et al.* have used the invariance of the rotational distributions for several different $NeCl_2$ dissociation channels to discount a classical scattering approach to vibrational predissociation of rare gas–halogen complexes and to suggest that the Franck–Condon model might have some validity.[28] On the other hand, Drobits and Lester have used the variation of the fragment rotational distributions from NeICl with initial vibrational level to conclude that classical scattering ideas have significant power in describing the disposal of energy into the fragments.[24] Our results suggest that neither of these conclusions is justified. The invariance of our distributions, calculated using classical mechanics, demonstrates that classical models do not always give rise to scaling of rotational distributions with E_{avl} and that conclusions based on the presence or absence of such scaling may be misleading.

This point is further amplified in Fig. 12, in which calculated values of j_{max} are plotted vs $E_{avl}^{1/2}$ for the two classical approximations used in our work. For purely impulsive scattering, we find that, as expected, j_{max} scales linearly with $E_{avl}^{1/2}$ for all values of E_{avl}. When we propagate classical trajectories on the model potential energy surface, however, we see that j_{max} is relatively insensitive to E_{avl} for the range of energies that are generally experienced ($E_{avl}\leqslant 100$ cm^{-1} or $E_{avl}^{1/2}\leqslant 10$ $cm^{-1/2}$) in the dissociation of Ne–halogen complexes. Indeed only for energies greater than several hundred wavenumbers is a linear dependence on $E_{avl}^{1/2}$ recovered for the classical trajectory model. In our $NeBr_2$ potential, the well depth is 83.9 cm^{-1}. The results presented in Fig. 12 suggest that E_{avl} must be larger than five times the well depth

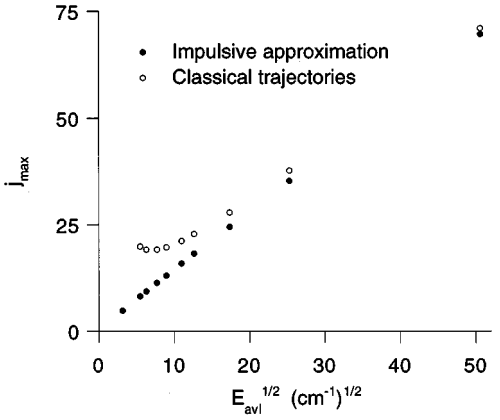

FIG. 12. Calculated variation of j_{max} on $E_{avl}^{1/2}$ for two classical models for the dissociation of $NeBr_2$. The angular momentum, j_{max}, is plotted in units of $\hbar$.

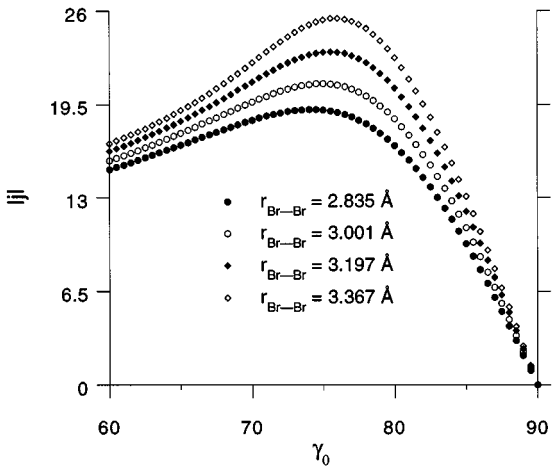

FIG. 13. Classical excitation functions for four values of Br–Br interatomic separation calculated using the classical trajectory model. E_{avl} is fixed at 67.7 cm^{-1}. The initial Ne–Br_2 angle γ_0 is plotted in degrees. The magnitude of the angular momentum, $|j|$, is plotted in units of $\hbar$.

before one would expect a classical energy scaling law to have validity.

The significant difference in the classical models that we have explored is the impact of the anisotropy associated with the potential well, which explicitly affects the classical trajectory results, but is explicitly ignored in the purely impulsive model. Within the classical trajectory model, when the recoiling fragments sample the anisotropy of the potential, there appears to exist a *minimum* amount of fragment rotational excitation that will occur, regardless of the value of E_{avl}. For the case displayed in Fig. 12, this minimum amount corresponds to $j_{max} \approx 19$. This observation provides further insight into the erratic behavior exhibited for low values of E_{avl}, as in Figs. 9 and 10. The orbiting behavior whose signature is displayed there occurs when the value of E_{avl} is smaller than that consistent with the minimum value of j_{max} dictated by the inherent anisotropy of the potential.

One of the problematic areas in assessing the validity of classical models is that detailed comparison with experimental data is difficult because of poor control over experimental variables. In Fig. 12, we have shown data calculated for the same potential energy surface and fragment rotational constant, but different values of E_{avl}. Experimentally, one varies E_{avl} by judicious choice of initial vibrational level such that a range of values of E_{avl} are sampled (Table I). This strategy is problematic, however, since in our model $NeBr_2$ potential surface, the potential energy is parametrically dependent on the average Br–Br bond length. Thus, the surface supported by Br_2 in the $v=9$ level is different from that supported by Br_2 in $v=14$ due to the anharmonicity of the Br–Br potential. By using different dissociation channels as a proxy for variation in E_{avl} we in fact confuse two quite different effects on the calculated rotational distributions. (A third effect, variation in the Br_2 fragment rotational constant with vibrational level, can be shown to have only a very small impact.) In Fig. 13, we show the classical excitation functions that result from varying the Br–Br bondlength while holding E_{avl} constant at 67.7 cm^{-1}. The range of r_{Br-Br} values selected correspond to the average Br_2 bondlengths for $v=9$ to $v=26$. The effect on j_{max} of varying the potential through its parametric dependence on bondlength is seen to be greater than that associated with E_{avl} alone! Specifically, the classical trajectory approach predicts a variation of j_{max} from 19 to 25 over this range of r_{Br-Br} values, with greater fragment rotational excitation associated with larger Br–Br distances. This effect can be traced to the greater anisotropy of the potential surface as the Br atoms separate; when $r_{Br-Br}=0$, for example, the potential is completely isotropic since the individual atom–atom Ne–Br Morse potentials have no angular dependence.

We can now understand the similarities in the calculated rotational distributions for $v=9$ and $v=14$ Br_2 fragments (Fig. 11). The available energy changes from 67.7 cm^{-1} ($v=9$ fragments) to 48.7 cm^{-1} ($v=14$ fragments). Examination of Fig. 12 suggests that this change should result in a slight decrease in the fragment rotational excitation for $v=14$ fragments. The average Br–Br bondlength increases, however, from 2.835 Å ($v=9$) to 2.947 Å ($v=14$), which favors increased rotational excitation for $v=14$ fragments (Fig. 13). The result is an approximate balance between these trends and a rotational distribution that is nearly identical for the two dissociation channels.

We can now turn to a comparison of the adequacy of the classical trajectory approach for the vibrational predissociation of $NeBr_2$ and NeIBr. Our analysis reveals that the classical trajectory method takes into account the fragment rotational excitation that arises from a combination of interactions with the repulsive and attractive parts of the potential energy surface. When E_{avl} is high, the dominant effect is the impulsive ''kick'' provided to the fragments as they scatter from the repulsive wall of the potential. When E_{avl} is low, the dominant interaction is with the anisotropic, attractive part of the potential, which provides a minimum value for the degree of fragment rotational excitation. For our $NeBr_2$ and NeIBr experiments, E_{avl} is relatively low and the latter effect is more important. Our experimental data in this regime suggests that the breadth of the rotational distribu-

tions are limited by energetic constraints. The breadth of the calculated distributions, however, are limited by the amount of angular momentum that can be transferred given the anisotropy of the potential energy surface. The agreement of the calculated distribution with the IBr fragment data appears so satisfying because these two constraints intersect for the particular dissociation channel that was the focus of our previous work, namely the detection of $v=11$ IBr fragments following the dissociation of $v=12$ NeIBr.[35] Indeed, complexes excited to higher vibrational levels (i.e., lower values of E_{avl}) could not be addressed in our computations, as the ''orbiting'' phenomena described previously was observed in the trajectory calculations. As noted earlier, this observation corresponds to a regime in which the potential provides for a larger degree of angular momentum excitation than is consistent with E_{avl}. Further, for NeIBr, complexes excited to lower vibrational levels (i.e., higher values of E_{avl}) could not be addressed experimentally, due to very unfavorable Franck–Condon factors and pump laser wavelengths ($\lambda > 735$ nm for $v<12$ in the A state of IBr).

In this context, the relatively poor showing for the classical trajectory method for the case of $NeBr_2$ can be interpreted as arising from the limited anisotropy of the potential given the total amount of energy for fragment rotational excitation. Clearly one solution to this discrepancy is to suggest that the model potential is inappropriate and that the true potential has substantially larger anisotropy. This could be the case, but any such revised potential must be consistent with the experimentally determined $NeBr_2$ geometry and dissociation energy, both of which are well represented by the current model potential. In addition, the form of our potential is one that has been found to generate reasonable agreement with experiment when used in quantum dynamics simulations of other rare gas–halogen complexes.[8,9,12,13] A more likely explanation is that one or more of the assumptions explicitly made to adopt the classical model is inappropriate, including the restriction that the total angular momentum, J, is 0 and the complete omission of the detailed mechanism of intramolecular vibrational coupling that is the predicate to the actual dissociation. Regardless of the origin of the discrepancy, it is clear that the fragments are capable of absorbing more angular momentum than simple classical interpretations of the anisotropy of the potential energy surface can accommodate. Obviously the classical models considered here will be less than satisfactory whenever the kinematics of angular momentum transfer do not dominate the dynamics. For several of the Ne–halogen complexes it appears that energy is the dominant constraint. Given our discussion above, it is not surprising that the agreement with the classical models is far from perfect. Quantum dynamics simulations carried out on the model $NeBr_2$ potential energy surface may illuminate the source(s) of the disparity and will serve an important role in determining the limits of the application of classical notions to the dissociation of rare gas–halogen van der Waals molecules.

ACKNOWLEDGMENTS

The research has been supported by a grant from the National Science Foundation (CHE-9223565). T.A.S. is grateful for the continuing support of the Camille and Henry Dreyfus Foundation in the form of a Henry Dreyfus Teacher-Scholar Award.

[1] R. Schinke, Annu. Rev. Phys. Chem. **39**, 39 (1988).
[2] M. I. Lester, Adv. Chem. Phys. **96**, 51 (1996).
[3] See, for example, K. C. Janda, Adv. Chem. Phys. **60**, 201 (1985); K. C. Janda and C. R. Bieler, in *Atomic and Molecular Clusters*, edited by E. R. Bernstein (Elsevier, Amsterdam, 1990), p. 455.
[4] J. A. Beswick and J. Jortner, Adv. Chem. Phys. **47**, 363 (1981).
[5] O. Roncero, J. A. Beswick, N. Halberstadt, P. Villarreal, and G. Delgado-Barrio, J. Chem. Phys. **92**, 3348 (1990).
[6] N. Halberstadt, S. Serna, O. Roncero, and K. C. Janda, J. Chem. Phys. **97**, 341 (1992).
[7] N. Halberstadt, J. A. Beswick, and K. C. Janda, J. Chem. Phys. **87**, 3966 (1987).
[8] R. L. Waterland, M. I. Lester, and N. Halberstadt, J. Chem. Phys. **92**, 4261, (1990).
[9] S. K. Gray and C. E. Wozny, J. Chem. Phys. **94**, 2817 (1991).
[10] N. Halberstadt, J. A. Beswick, O. Roncero, and K. C. Janda, J. Chem. Phys. **96**, 2404 (1992).
[11] N. Halberstadt, O. Roncero, and J. A. Beswick, Chem. Phys. **129**, 83 (1989).
[12] J. A. Beswick and G. Delgado-Barrio, J. Chem. Phys. **73**, 3653 (1980).
[13] O. Roncero, J. A. Beswick, N. Halberstadt, P. Villarreal, and G. Delgado-Barrio, J. Chem. Phys. **92**, 3348 (1990).
[14] G. E. Ewing, J. Phys. Chem. **91**, 4662 (1987).
[15] A. A. Buchachenko, A. Y. Balsogolov, and N. F. Stepanov, J. Chem. Soc. Faraday Trans. **90**, 3229 (1994).
[16] S. S. Huang, C. R. Bieler, K. C. Janda, F-M. Tao, W. Klemperer, P. Casavecchia, G. G. Volpi, and N. Halberstadt, J. Chem. Phys. **102**, 8846 (1995).
[17] O. Roncero, P. Villarreal, G. Delgado-Barrio, N. Halberstadt, and K. C. Janda, J. Chem. Phys. **99**, 1035 (1993).
[18] O. Roncero and S. K. Gray, J. Chem. Phys. **104**, 4999 (1996); S. K. Gray and O. Roncero, J. Phys. Chem. **99**, 2512 (1995).
[19] O. Roncero, N. Halberstadt, and J. A. Beswick, J. Chem. Phys. **104**, 7554 (1996).
[20] D. H. Levy, Adv. Chem. Phys. **47**, 323 (1981).
[21] J. C. Drobits, J. M. Skene, and M. I. Lester, J. Chem. Phys. **84**, 2896 (1986).
[22] J. M. Skene, J. C. Drobits, and M. I. Lester, J. Chem. Phys. **85**, 2329 (1986).
[23] J. C. Drobits and M. I. Lester, J. Chem. Phys. **88**, 120 (1987).
[24] J. C. Drobits and M. I. Lester, J. Chem. Phys. **89**, 4716 (1988).
[25] R. L. Waterland, J. M. Skene, and M. I. Lester, J. Chem. Phys. **89**, 7277 (1988).
[26] J. I. Cline, B. P. Reid, D. D. Evard, N. Sivakumar, N. Halberstadt, and K. C. Janda, J. Chem. Phys. **89**, 3535 (1988).
[27] W. D. Sands, C. R. Bieler, and K. C. Janda, J. Chem. Phys. **95**, 729 (1991).
[28] J. I. Cline, N. Sivakumar, D. D. Evard, C. R. Bieler, B. P. Reid, N. Halberstadt, S. R. Hair, and K. C. Janda, J. Chem. Phys. **90**, 2605 (1989).
[29] S. R. Hair, J. I. Cline, C. R. Bieler, and K. C. Janda, J. Chem. Phys. **90**, 2935 (1989).
[30] D. D. Evard, C. R. Bieler, J. I. Cline, N. Sivakumar, and K. C. Janda, J. Chem. Phys. **89**, 2829 (1988).
[31] C. R. Bieler, D. D. Evard, and K. C. Janda, J. Phys. Chem. **94**, 7452 (1990).
[32] C. R. Bieler, K. E. Spence, and K. C. Janda, J. Phys. Chem. **95**, 5058 (1991).
[33] D. G. Jahn, S. G. Clement, and K. C. Janda, J. Chem. Phys. **101**, 283 (1994).
[34] D. G. Jahn, W. S. Barney, J. Cabalo, S. G. Clement, A. Rohrbacher, T. J. Slotterback, J. Williams, K. C. Janda, and N. Halberstadt, J. Chem. Phys. **104**, 3501 (1996).
[35] T. A. Stephenson, J. Chem. Phys. **97**, 6262 (1992).

[36] B. A. Swartz, D. E. Brinza, C. M. Western, and K. C. Janda, J. Phys. Chem. **88**, 6272 (1984).
[37] F. Thommen, D. D. Evard, and K. C. Janda, J. Chem. Phys. **82**, 5295 (1985).
[38] J. I. Cline, D. D. Evard, B. P. Reid, N. Sivakumar, F. Thommen, and K. C. Janda, in *Structure and Dynamics of Weakly Bound Molecular Complexes*, edited by A. Weber (Reidel, Dordrecth, 1987), pp. 533–551.
[39] N. Sivakumar, J. I. Cline, C. R. Bieler, and K. C. Janda, Chem. Phys. Lett. **147**, 561 (1988).
[40] P. Berwanger, K. S. Viswanathan, and J. Tellinghuisen, J. Mol. Spectros. **91**, 275 (1982).
[41] W. R. Simpson and T. A. Stephenson, J. Chem. Phys. **90**, 3171 (1989).
[42] S. A. Walter and T. A. Stephenson, J. Chem. Phys. **96**, 3536 (1992).
[43] See, for example, R. Vasudev, R. Zare and R. N. Dixon, J. Chem. Phys. **80**, 4863 (1984); P. Andresen, G. S. Ondrey, B. Titze and E. Rothe, *ibid*. **80**, 2548 (1984).
[44] R. F. Barrow, T. C. Clark, J. A. Coxon, and K. K. Yee, J. Mol. Spectros. **51**, 428 (1974).
[45] L. Beneventi, P. Casavecchia, G. G. Volpi, C. R. Bieler, and K. C. Janda, J. Chem. Phys. **98**, 178 (1993).
[46] F.-M. Tao and W. Klemperer, J. Chem. Phys. **97**, 440 (1992).
[47] G. Chalasinski, M. Gutowski, M. M. Szczesniak, J. Sadlej, and S. Scheiner, J. Chem. Phys. **101**, 6800 (1994).
[48] J. Sadlej, G. Chalasinski, and M. M. Szczesniak, J. Mol. Struc. (Theochem) **307**, 187 (1994).
[49] J. Sadlej, G. Chalasinski, and M. M. Szczesniak, J. Chem. Phys. **99**, 3700 (1993).
[50] K. C. Janda, O. Roncero, and N. Halberstadt, J. Chem. Phys. **105**, 5830 (1996).
[51] B. P. Reid, K. C. Janda, and N. Halberstadt, J. Phys. Chem. **92**, 587 (1988).
[52] M. D. Morse, K. F. Freed, and Y. B. Band, J. Chem. Phys. **70**, 3604 (1979); M. D. Morse and K. F. Freed, *ibid*. **78**, 6045 (1983).
[53] R. Schinke, J. Chem. Phys. **85**, 5049 (1986).
[54] D. W. Noid, S. K. Gray, and S. A. Rice, J. Chem. Phys. **84**, 2649 (1986).